Ceramics International 44 (2018) 953–958

Contents lists available at ScienceDirect

Ceramics International

journal homepage: www.elsevier.com/locate/ceramint

Microwave-assisted hydrothermal synthesis followed by heat treatment: A new route to obtain $CaZrO_3$

Wagner D. Macedo Jr.[a,*], Agda E. Souza[a], Gleyson T.A. Santos[a], Silvio R. Teixeira[a], Elson Longo[b]

[a] São Paulo State University (UNESP), Dept. of Physics, Presidente Prudente, São Paulo 19060-900, Brazil
[b] Federal University of São Carlos (UFSCar), CDMF/CEPID, São Carlos, São Paulo 13565-905, Brazil

ARTICLE INFO

Keywords:
Hydrothermal
Microwave
Heat treatment
$CaZrO_3$

ABSTRACT

$CaZrO_3$ nanoparticles were obtained by a new synthesis route: nucleation using the microwave-assisted hydrothermal method (MAH) and crystallization by heat treatment. Structural characterization by X-ray diffraction (XRD) was performed for the synthesized material and after heat treatment at 700, 800, 900, 1000 and 1200 °C. At 800 °C, the lakargite phase crystallization ($CaZrO_3$) starts and portions of the non-stoichiometric calcium-zirconium oxide phase were observed by XRD and Raman spectroscopy. A residual $CaCO_3$ phase was present in the untreated samples. At 1200 °C, the well-crystallized stoichiometric and non-stoichiometric mixed oxide phases of $CaZrO_3$ (crystallites of about 75 nm) were observed, along with particle agglomerates often in the micrometer range. The synthesized material was subjected to differential thermal analysis, which revealed carbonate degradation at approximately 695 °C, resulting in a small loss of mass of 6%. An endothermic reaction at 85 °C was observed for water loss, where there was a considerable amount of energy involved. This result showed the sensitivity to moisture absorption and adsorption processes of the $CaZrO_3$ sample, obtained by the MAH route. UV–Vis spectroscopy showed the characteristic gap energies for the two phases, which were 2.9 (non-stoichiometric) and 4.9 eV (stoichiometric), values smaller than those obtained by usual synthesis routes.

1. Introduction

Calcium zirconate ($CaZrO_3$) is a perovskite family ceramic, whose mineral in its natural form was only discovered in 2008 in the northern part of the Caucasus region, Russia [1]. This material shows polymorphic transition from orthorhombic to cubic at 1750 °C, has a relatively small thermal expansion coefficient and high thermal and chemical stability [2]. At room temperature, its orthorhombic structure exhibits slightly deformed [ZrO_6] and [CaO_8] clusters (Fig. 1), which may generate intermediate states in the energy gap of the material, affecting its optical properties [3].

$CaZrO_3$ has very interesting electrical properties, potentiating its use in various applications, mainly as a humidity sensor [5]. Dudek et al. [6] reported the sensor properties of a $CaZrO_3$-CaO-ZrO_2 system, obtained by different synthesis methods with subsequent thermal treatments at temperatures between 1000 and 1500 °C. $CaZrO_3$ can be used as a semiconductor, with applications in high-temperature water sensors, photoluminescent emitter at 450 and 700 nm, solid electrolyte, proton conductor and photocatalytic material (for molecules such as rhodamine B) [5–10]. In addition, $CaZrO_3$ can be used in various areas due to its refractory character (melting point of 2340 °C), relative high electrical permittivity and low dissipation factor [11].

Stoichiometric $CaZrO_3$ has been reported as a p-type semiconductor material. When small excesses of CaO or ZrO_2 are added to $CaZrO_3$, ionic conductivity is observed for different values of oxygen partial pressure besides high chemical stability at temperatures above 1000 °C. Therefore, $CaZrO_3$-ZrO_2 heterostructure can be beneficial for both ionic conduction and improvements in water adsorption due to its increased surface area [12].

There are several physical or chemical methods for obtaining this material, such as the polymer precursor, or Pechini method [13], sol-gel [14], gelation-combustion [15], solid state reaction [16] and microwave-assisted salt melting [17]. However, there are no reported studies on the synthesis of this material by microwave-assisted hydrothermal methods (MAH) [18]. In this work, $CaZrO_3$ nanoparticles were nucleated using MAH and subsequently thermally treated to complete the $CaZrO_3$ phase crystallization. A new method for the synthesis of this ceramic allows us to investigate new microstructures and possibly improve their properties, especially those concerning applications in humidity sensors [19].

* Correspondence to: Roberto Simonsen, 305, Presidente Prudente, São Paulo 19060-900, Brazil.
E-mail address: snow_dias@hotmail.com (W.D. Macedo).

http://dx.doi.org/10.1016/j.ceramint.2017.10.028
Received 18 July 2017; Received in revised form 3 October 2017; Accepted 7 October 2017
Available online 09 October 2017

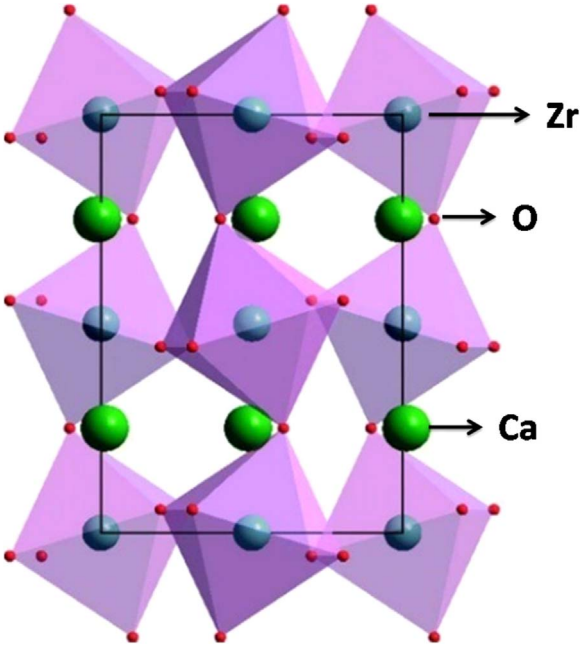

Fig. 1. [ZrO_6] and [CaO_8] clusters slightly deformed in the $CaZrO_3$ orthorhombic structure [4].

2. Experimental procedure

$CaZrO_3$ nanoparticles were produced in two processing steps. In the first, we used MAH with a heating rate of 140 °C/min, temperature of 140 °C, synthesis times of 20 and 160 min and maximum pressure of 4 bar. The precursor solution was prepared in deionized water by adding, with stirring, $CaCl_2{\cdot}2H_2O$ (99%, Synth), $ZrOCl_2{\cdot}8H_2O$ (99%, Synth) and NaOH (6 mol/L) (98%, Synth) as a mineralizing agent. The chlorides were stoichiometrically mixed at a 0.01 mol Ca/Zr ratio. After the synthesis, the supernatant was discarded and the ceramic precipitate was washed several times with deionized water until neutral pH [20]. The material thus synthesized was dried in an oven, ground in an agate mortar and then subjected to structural characterization. In the second stage, the samples were subjected to thermal treatments at 700, 800, 900, 1000 and 1200 °C for 1 h, using a laboratory furnace (EDG 3000). To evaluate the effect of heating time, a sample was treated at 1000 °C for 6 h.

Identification of the phases in the samples was performed by X-ray diffraction (XRD) analysis (Shimadzu XRD-6000), with Cu Kα1 (λ = 1.5406 Å) and Cu Kα2 (λ = 1.5444 Å), at 40 kV and 30 mA, with 0.02° step, scanning speed of 2°/min and angular range 2θ = 10° to 80°. Also, data were collected for structure refinement using the Rietveld method, for the $CaZrO_3$ sample heated at 1200 °C. In this case, the angular range (2θ) was from 10° to 120°, with scanning speed of 0.2°/min. The average crystallite size of some samples was calculated using the Scherrer equation (Eq. (1)), using XPowder software, where background and $k\alpha 2$ radiation were subtracted. In this equation, D is the average crystallite size, k is a dimensionless constant called the form factor (Scherrer constant, which varies with the geometric configuration of the crystallite), λ is the wavelength of the radiation (Cu $k\alpha 1$), θ is the diffraction angle, and β is the full width at half maximum (FWHM) of the most intense diffraction peak [21].

$$D = k\lambda/\beta cos\theta \quad (1)$$

Thermal characterization was performed by differential scanning calorimetry (DSC) and thermogravimetry (TG) (SDT-Q600TA Instruments). The analyses were carried out up to 1200 °C, at a heating rate of 10 °C/min in air flow (100 mL/min). The morphology of the synthesized (160 min) and heated sample (1000 °C, 1 h) were characterized using a scanning electron microscope (SEM, Supra™ 35 Gemini, Zeiss).

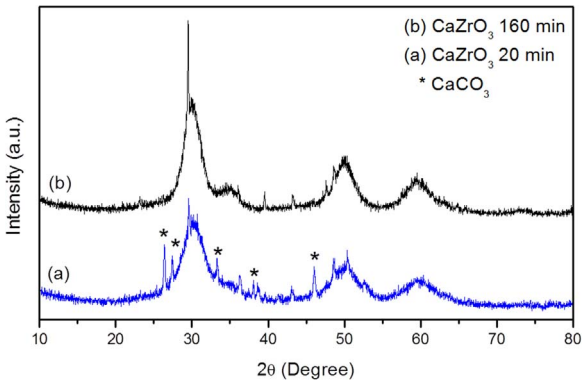

Fig. 2. XRD of the $CaZrO_3$ samples synthesized for (a) 20 min and (b) 160 min (140 °C) using MAH method.

The synthesized sample (MAH) at 160 min and treated (1200 °C, 1 h) was analyzed directly in the powder form at room temperature using Raman scattering and UV–Vis absorption. Raman spectroscopy was performed using a Renishaw micro-Raman, inVia model, equipped with Leica microscope and CCD detector. Raman spectra were obtained with scanning from 100 to 600 cm^{-1}, with a 514 nm wavelength excitation laser (He-Ne). Finally, UV–Vis spectroscopy was performed by diffuse reflectance (Cary 5 G Varian) spectrophotometer (UV–Vis–NIR) in full reflection mode. The equipment was calibrated with two Labsphere reflectance standards, SRS 94-010 (white, 99% reflection) and SRD 02–010 (black, 0.2% reflection). The region analyzed was 800–200 nm with a 600 nm/min step and a lamp change (visible - ultraviolet) at 350 nm. The gap energy (E_{gap}) was estimated using the Wood and Tauc method [22].

3. Results and discussion

The X-ray diffractograms of samples synthesized by MAH for 20 and 160 min (Fig. 2) showed wide peaks (at 30°, 50° and 60°, 2θ). This particular characteristic of wide peaks is related to the short- and medium-range order of the ceramic material structure, indicating a process of phase nucleation. The wide peak between 20° and 40° (2θ), with a maximum of 30°, is characteristic of the medium-range order of a glass structure. These three peaks are located in the positions of the most intense peaks of non-stoichiometric calcium-zirconium oxide. The peak near 2θ = 30° corresponds to the calcium zirconate phase. In addition, calcium carbonate formation ($CaCO_3$ – PDF 5-0586) can be observed, mainly for the sample prepared with less synthesis time (20 min). In this case, it can be concluded that the MAH method used provides energy for the crystallite nucleation process, but that it is not sufficient for phase growth.

Fig. 3 shows the thermal analysis results of the oven-dried $CaZrO_3$ ceramic powder, synthesized by MAH for 20 min. The endothermic peak at 85 °C showed a mass loss of 8%, associated with loss of surface water (adsorbed water). Another endothermic peak, at 695 °C (loss of approximately 6% mass), was related to calcium carbonate degradation, as observed in the X-ray diffractogram of this sample (Fig. 2). In general, carbonate decomposition occurred near 900 °C [23,24]; however, the lower value observed was associated with the size of the particles, i.e., the smaller the size, the lower the decomposition temperature. Above 700 °C, other reactions occurred without change in mass, and therefore, there was no degradation of the material.

Since the longer synthesis time (MAH) resulted in a material with lower carbonate volume, the thermal treatments for phase crystallization were performed only with the sample synthesized for 160 min. Small amounts of this sample were heated at four different temperatures (700, 800, 900 and 1000 °C) for one hour and analyzed by XRD

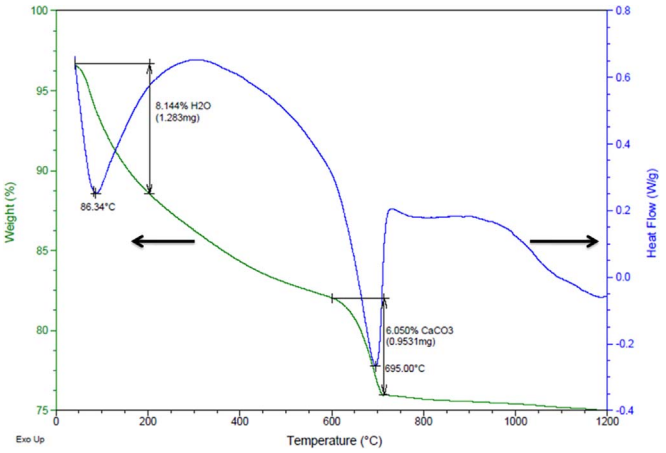

Fig. 3. Thermogram of the $CaZrO_3$ sample synthesized for 20 min.

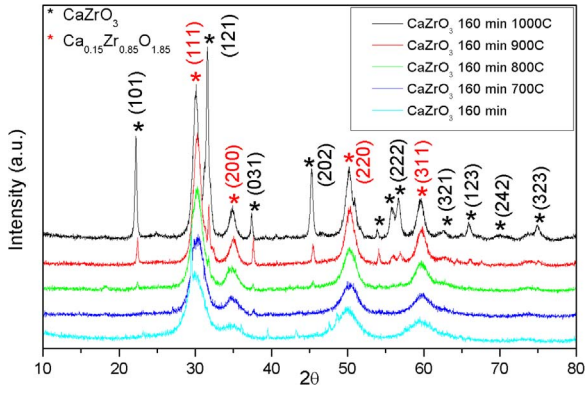

Fig. 4. XRD of the $CaZrO_3$ samples synthesized by MAH for 160 min (a) without heating, and heated at (b) 700 °C, (c) 800 °C, (d) 900 °C and (e) 1000 °C, for 1 h.

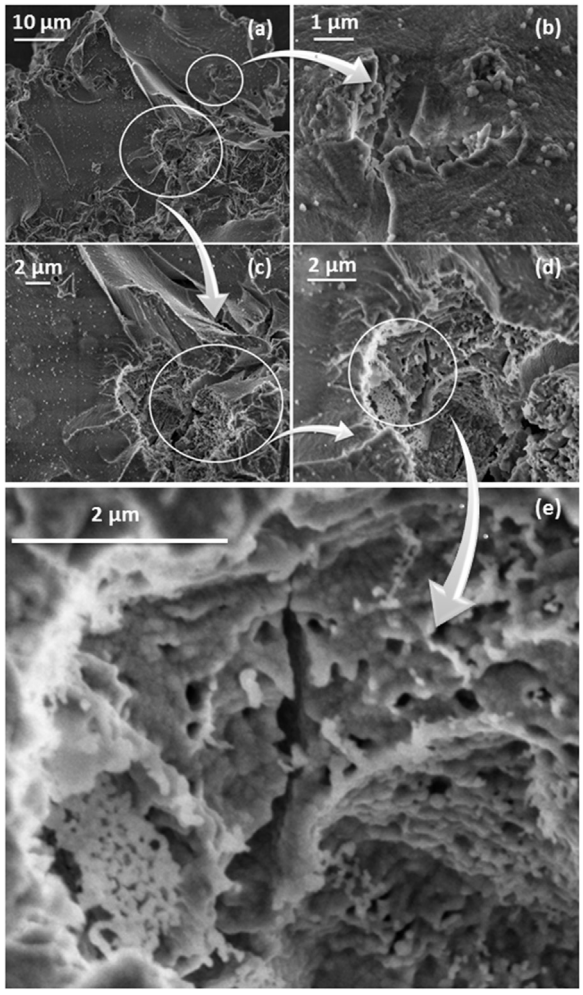

Fig. 5. SEM images of the $CaZrO_3$ sample synthesized by MAH for 160 min and heated at 1000 °C for 1 h.

(Fig. 4). The sample heated at 700 °C showed little change in the diffractogram. The XRD peaks became more intense and sharper, especially those near 30°. In this sample, the carbonate fine peaks were not observed, confirming the thermal analysis results (Fig. 3), i.e., calcium carbonate decomposition occurred at this temperature. The diffractogram showed that in the samples heated at 800 and 900 °C, the initial growth of the calcium zirconate (lakargite, PDF 35-790 – $CaZrO_3$) and non-stoichiometric calcium-zirconium oxide phases (PDF 26-341 – $Ca_{0.15}Zr_{0.85}O_{1.85}$) was observed, but that they did not crystallize completely. The larger diffraction peaks, close to 30°, 35°, 50° and 60° (2θ) are characteristic of the non-stoichiometric calcium-zirconium oxide phase, with cubic unit cell, while the sharp ones are characteristic of the orthorhombic calcium zirconate phase. Therefore, with these synthesis conditions and heating, non-stoichiometric calcium-zirconium oxide nanoparticles were predominantly formed and well-crystallized calcium zirconate, characterized by fine XRD peaks, was less evident. However, as the heat treatment temperature was increased (1000 °C), there was an increase in the $CaZrO_3$ phase over the non-stoichiometric phase.

The SEM images for the sample synthesized for 160 min and treated at 1000 °C are shown in Fig. 5. The images show agglomerates (micrometric) with high roughness and no defined shapes (Fig. 5 (a)) and with nanometric particles adhered to their surface (Fig. 5 (a)–(d)), which is usually observed in the growth of perovskite crystals [25]. The observation of agglomerate particles with undefined morphology indicated that one hour of heat treatment was not sufficient for phase morphological evolution [17]. The X-ray diffractograms showed wide peaks, especially for the non-stoichiometric phase, indicating smaller particles for this phase. These images showed different morphologies compared to those for other synthesis routes of $CaZrO_3$ [5,6], which although they showed that the samples were composed of porous agglomerates, there were smaller particles with defined morphology. This characteristic is observed in the enlargement in Fig. 5(d), which shows that the micrometric particle analyzed was formed by the agglomeration of nanometric particles, apparently spherical and organized to give a porous microstructure (Fig. 5(e)).

Huang et al. [17] and other authors [26,27] report that a longer heating time is more efficient than a higher temperature in the crystallization of zirconates. Accordingly, a sample synthesized for 160 min by MAH was heated at 1000 °C for 6 h (Fig. 6 – (I)). For this longer heating time, there was a slight improvement in the crystallization of the two phases, which showed more defined XRD peaks. Although this slight improvement in the intensity and resolution of the doublets, at 30° and between 50° and 60° (2θ) confirmed a better phase crystallization in the sample treated for 6 h, these changes were not as substantial as those observed by Huang et al. [17].

For the sample treated at 1200 °C for 1 h, the X-ray diffraction pattern (Fig. 6 – (II)) showed the existence of two well-ordered phases, with sharp and more intense diffraction peaks. This showed that the higher temperature was more effective than longer heat treatment time (Fig. 6 – (I)) in the crystallization process for this synthesis method. For this sample, structure refinement was performed using the Rietveld method (Fig. 7). From the refinement, the lattice parameters and percentage of formed phases were obtained. The mean crystallite size was obtained by the Scherrer equation using XPowder software (Table 1).

Refinement showed good values of convergence parameters between the points observed and calculated (χ^2 = 1.785, wRp = 8.44%,

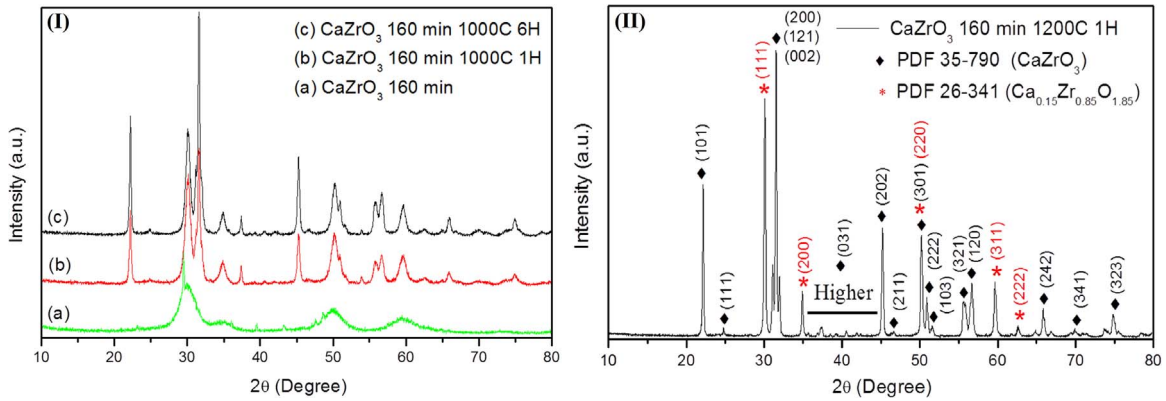

Fig. 6. (I) XRD of $CaZrO_3$ samples synthesized by MAH for 160 min: sample (a) without heat treatment; (b) heated at 1000 °C for 1 h, (c) at 1000 °C for 6 h and (II) 1200 °C for 1 h.

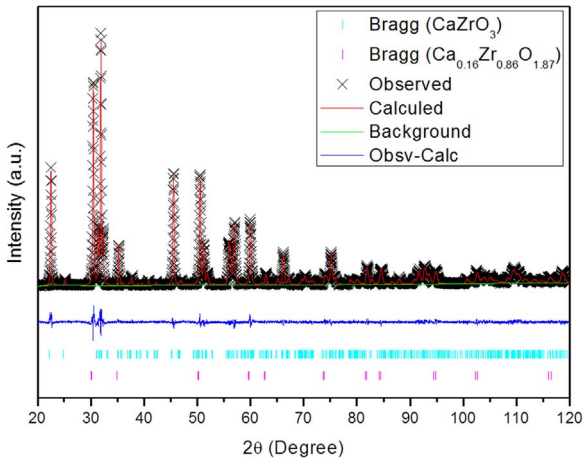

Fig. 7. Rietveld structure refinement diffractogram of the $CaZrO_3$ sample synthesized by MAH for 160 min and heated at 1200 °C for 1 h.

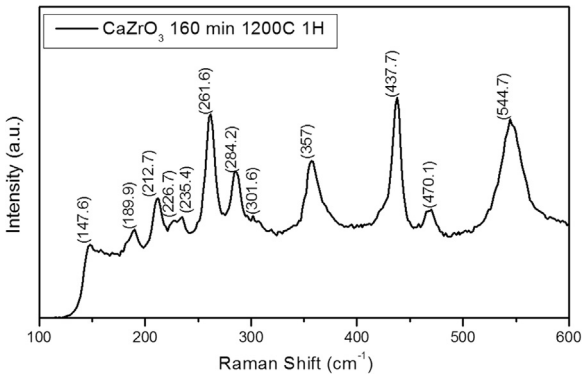

Fig. 8. Raman spectrum of the $CaZrO_3$ sample synthesized by MAH for 160 min and heated at 1200 °C for 1 h.

$R(F^2)$ = 3.67%). The percentages of the orthorhombic calcium zirconate and non-stoichiometric calcium-zirconium oxide cubic phases were 65% and 35%, respectively. The cubic phase stoichiometry was determined to be $Ca_{0.16}Zr_{0.86}O_{1.87}$. The diffractograms demonstrated that with heat treatment, the non-stoichiometric phase was initially more crystalline, i.e., larger crystallites, with more intense diffraction peaks. According to the average crystallite size before (4 and 52 nm) and after (76 and 75 nm) heat treatment at 1200 °C, zirconate crystallization rate was higher than that of non-stoichiometric oxide, during heat treatment. Both phases reached approximately the same final crystallite sizes, as observed in Fig. 6 – (II) by the peak width of each phase. Comparing the calculated lattice parameters with those of the reference diffractograms (PDF), there was a slight increase in unit cell for the two phases.

The Raman spectroscopy results of the heated sample at 1200 °C are shown in Fig. 8 and Table 2, confirming the X-ray diffraction data. The most evident and intense vibration modes were those referring to the $CaZrO_3$ phase. Non-stoichiometric phase vibration modes, such as those peaking at 141 and 460 cm^{-1}, coincided with those of the calcium zirconate phase [28]. The other peaks were very weak and overlapped by calcium zirconate vibrational modes. According to Rosa et al. [13], the frequencies near 141 and 185 cm^{-1} correspond to the A_g and B_{2g}

Table 2
Comparison of the wave numbers obtained for the $CaZrO_3$ sample synthesized by MAH for 160 min and heated at 1200 °C for 1 h with those of reference 29.

$CaZrO_3$ Sample (cm^{-1})	Orera et al. [29] (cm^{-1})	Assigned Mode
147.6	145	(A_g) Network Mode
189.9	190	(B_{2g}) Zr-O Flexion
212.7	212	(B_{2g}) Zr-O Flexion
226.7	227	($B_{1g\ or}B_{3g}$) Zr-O Flexion
235.4	234	(B_{2g}) Zr-O Flexion
261.6	262.5	(A_g) Zr-O Flexion
284.2	286.5	(A_g) Zr-O Flexion
301.6	305	($B_{1g\ or}B_{3g}$) Zr-O Twist
357	358	(A_g) Twist
–	418	(B_{2g}) Twist
437.7	439	($A_g + B_{1g}$) Twist
470.1	469	(B_{2g}) Zr-O Stretching
544.7	543	($A_g + B_{2g}$) Zr-O Stretching
–	547	($B_{1g} + B_{3g}$) Zr-O Stretching

Table 1
Rietveld structure refinement data of the $CaZrO_3$ sample synthesized by MAH for 160 min and heated at 1200 °C for 1 h.

Phase		Structure	a (Å)	b (Å)	c (Å)	Weight % (%wt)	Average crystallite size (nm)
$CaZrO_3$		Orthorhombic	5.599	8.019	5.752	65%	76
$Ca_{0.16}Zr_{0.86}O_{1.87}$		Cubic	5.139	5.139	5.139	35%	75
PDF*	$CaZrO_3$	Orthorhombic	5.593	8.010	5.756	–	–
	$Ca_{0.15}Zr_{0.85}$ $O_{1.85}$	Cubic	5.135	5.135	5.135	–	–

* **Powder Diffraction Files**: 35-790 ($CaZrO_3$) and 26-341 ($Ca_{0.15}Zr_{0.85}$ $O_{1.85}$).

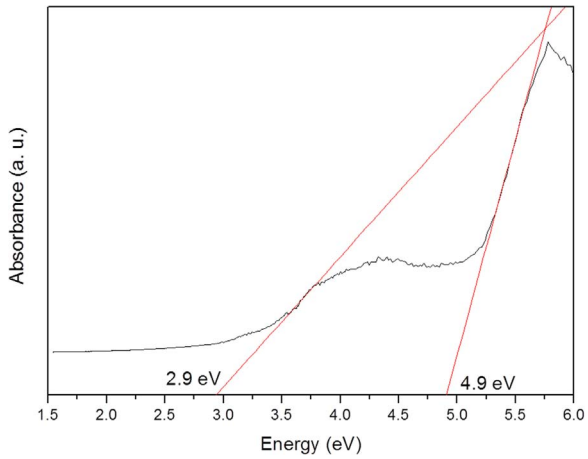

Fig. 9. UV–Vis absorption spectrum of the $CaZrO_3$ sample synthesized by MAH for 160 min and heated at 1200 °C for 1 h.

vibrational modes of the Zr-O bond, respectively. All other torsion modes, stretching and bending, peaked approximately in the same regions as the references [13–29]. The differences seen at the maximum point of these bands can be related to the average crystallite size of each sample, because the FWHM of Raman bands, in general, is inversely proportional to the average crystallite size [30]. On the other hand, the non-stoichiometric calcium-zirconium phase may contain structural defects due to oxygen vacancies, for example, which may change the bonding energy between Zr and O atoms and also the cluster $[ZrO_6]$ symmetry, which can result in the Raman mode shift. According to André [2], defects are related to short-, medium- and long-distance structural order-disorder, which in turn may alter the material electronic structure and surfaces and interfaces as well. As a consequence, changes in Raman band position and E_{gap} may occur, for example. Also, according to Li et al.[31], the bands at 149, 269 and 312 cm^{-1} are characteristic of the tetragonal ZrO_2 phase. However, the spectrum in Fig. 9 showed the absence of these bands, confirming the finding that the non-stoichiometric phase ($Ca_{0.16}Zr_{0.86}O_{1.87}$), whose substitution occurs at the Ca/Zr site, has cubic symmetry, as identified by XRD.

The optical E_{gap} of the $CaZrO_3$ sample synthesized by MAH for 160 min and heated at 1200 °C for 1 h was determined using the Wood and Tauc method [22], considering an indirect transition. Fig. 9 shows the absorption spectrum versus photon energy for this sample. Two absorption regions were observed, for which two different E_{gap} were estimated, 2.9 and 4.9 eV. These values were attributed to the gap of the non-stoichiometric calcium-zirconium and $CaZrO_3$ phases, respectively. In the work of Rosa et al. [13], the experimental E_{gap} value of the pure $CaZrO_3$ phase was 5.7 eV, while André [2] reported a value of 3.8 eV, also for a pure phase, where the polymeric precursor method was used in both cases. Stoch et al. [32] found E_{gap} values on the order of 4.1 eV for $CaZrO_3$, prepared by melting in an electric arc and the standard solid state reaction method. These results showed the influence of the synthesis method and suggested that the coexistence of non-stoichiometric calcium-zirconium and $CaZrO_3$ phases significantly alter the band structure configuration of each one. ZrO_2, for example, may have its E_{gap} changed by dopants, as observed by Lovisa [33]. According to the author, the controlled doping of ZrO_2 with Tb, Eu or Tm, associated with the calcination conditions, can alter E_{gap} from 2.8 to 4.8 eV. This author contends that the decrease in gap energy depends on structural ordering, that is, the lower the E_{gap} value, the greater the number of intermediate levels in the band gap. In this context, for the non-stoichiometric calcium-zirconium phase, the Ca/Zr substitution and the absence of oxygen in the lattice leads to medium-range defects and may induce destabilization of its electronic structure and alteration in E_{gap}. In addition, these changes in E_{gap}, compared to those in the literature for the two phases, may be related to the nanometric particle size and interface effects between them.

4. Conclusions

$CaZrO_3$ samples were obtained by a new synthesis route: nucleation using the MAH method and crystallization by heat treatment. The results showed that the crystallization process of the $CaZrO_3$ phase started with heating at 800 °C, together with the crystallization of the non-stoichiometric calcium-zirconium oxide. After heat treatment at 1200 °C, the sample consisted of 65% orthorhombic $CaZrO_3$ phase and 35% non-stoichiometric cubic phase, both with high structural ordering, according to XRD data and structure refinement. SEM images showed that after heat treatment at 1000 °C, the samples consisted of micrometric particles formed by the agglomeration of nanometric particles. Also, some nanoparticles were found to be adhered to the surface of larger particles. The material synthesized apparently exhibited sensitivity to surface water, as shown by the thermal analysis results, which might have been improved (relative to the single-phase $CaZrO_3$ materials) due to its coexistence with the non-stoichiometric phase and its consequent increase in surface area. The UV–Vis spectrum showed two absorption regions, for which the gap energy values of 2.9 and 4.9 eV were estimated, and attributed to the non-stoichiometric calcium-zirconium oxide and $CaZrO_3$ phases, respectively. These values are smaller than those obtained by other synthesis routes. Variations in the E_{gap} values for the two phases, compared to the literature, may be associated with structural disorder and with the interface between the nanometric particles of both phases.

Acknowledgements

The authors would like to thank Dr. A. Leyva (USA) for English editing of the manuscript.

This work was supported by FAPESP/CEPID [2013/07296-2], CNPq [573636/2008-7] and CAPES through a scholarship (PhD – POSMAT) awarded to W. D. Macedo Jr.

References

[1] E.V. Galuskin, V.M. Gazeev, T. Armbruster, A.E. Zadov, I.O. Galuskina, N.N. Pertzev, P. Dzierzanowski, M. Kadiyski, A.G. Gurbanov, R. Wrzalik, A. Winiarski, Lakargiite $CaZrO_3$: a new mineral of the perovskite group from the North Caucasus, Kabardino-Balkaria, Russia, Am. Mineral. 93 (2008) 1903–1910.
[2] R.S. André, Zirconato de Cálcio: Um Estudo Para Aplicação Como Sensor de Umidade Relativa. (Calcium Zirconate: A Study for Application as Relative Humidity Sensor) (Master's dissertation), Federal Universityof São Carlos, São Carlos, São Paulo, Brazil, 2013.
[3] V.M. Longo, A.T. Figueiredo, A.B. Campos, J.W. Espinosa, A.C. Hernandes, C.A. Taft, J.R. Sambrano, J.A. Varela, E. Longo, Different origins of green-light photoluminescence emission in structurally ordered and disordered powders of calcium molibdate, J. Phys. Chem. A 112 (2008) 8920.
[4] X. Yang, Q. Li, R. Liu, B. Liu, S. Jiang, K. Yang, J. Liu, Z. Chen, B. Zou, T. Cui, B. Liu, A novel pressure-induced phase transition in $CaZrO_3$, CrystEngComm. 16 (2014) 4441.
[5] R.S. André, S.M. Zanetti, J.A. Varela, E. Longo, Synthesis by a chemical method and characterization of $CaZrO_3$ powders: potential application as humidity sensors, Ceram. Int. 40 (2014) 16627–16634.
[6] M. Dudek, E.D. Ciesla, Some observations on synthesis and electrolytic properties of nonstoichiometric calcium zirconate, J. Alloy. Compd. 475 (2009) 846.
[7] C.C. Wang, S.A. Akbar, W. Chen, J.R. Schorr, High-temperature thermistors based on yttria and calcium zirconate, Sens Actuators A 58 (1997) 237–243.
[8] D. Janke, Oxygen probes based on calcia-doped hafnia or calcium zirconate for use in metallic melts, Metall. Mater. Trans. B 13 (1982) 227–235.
[9] A.H. Setiawan, J.W. Fergus, Preparation and characterization of In-doped $CaZrO_3$ as the electrolyte in hydrogen sensors for use in molten aluminum, Ceram. Trans. 130 (2002) 47–56.
[10] T. Yajima, K. Koide, H. Takai, N. Fukatsu, H. Iwahara, Application of hydrogen sensor using proton conductive ceramics as a solid electrolyte to aluminum casting, Solid State Ion. 79 (1995) 333–337.
[11] Y. Du, Z.P. Jin, P.Y. Huang, Thermodynamic calculation of the zirconia calcia system, J. Am. Ceram. Soc. 75 (1992) 3040–3048.
[12] S.C. Hwang, G.M. Choi, The effect of cation nonstoichiometry on the electrical conductivity of aceptor-doped $CaZrO_3$, Solid State Ion. 177 (2006) 3099.
[13] I.L.V. Rosa, M.C. Oliveira, M. Assis, M. Ferrer, R.S. André, E. Longo, M.F.C. Gurgel, A theoretical investigation of the structural and electronic properties of

orthorhombic $CaZrO_3$, Ceram. Int. 41 (2015) 3069–3074.
[14] J. Han, Z. Wen, J. Zhang, et al., Synthesis and characterization of proton conductive $CaZr_{0.90}In_{0.10}O_3$-delta by a citric acid complexation method, Fusion Eng. Des. 85 (2010) 2100.
[15] A.L. Ibiapino, L.P. Figueiredo, Síntese e caracterização de $CaZrO_3$ e $BaZrO_3$ nanoestruturados. (Synthesis and characterization of nanostructured $CaZrO_3$ and $BaZrO_3$), Quim. Nova. 36 (2013) 762–767.
[16] M.R. Nadler, E.S. Fitzsimmons, Preparation and properties of calcium zirconate, J. Am. Ceram. Soc. 38 (1955) 214–215.
[17] Z. Huang, X. Deng, J. Liu, S. Zhang, Preparation of $CaZrO_3$ powders by a microwave-assisted molten salt method, J. Ceram. Soc. Jpn. 124 (2016) 593–596.
[18] S. Komamerni, R. Roy, Q.H. Li, Microwave-hydrothermal synthesis of ceramic powders, Mater. Res. Bull. 27 (1992) 1393–1405.
[19] T.A. Blank, L.P. Eksperiandova, K.N. Belikov, Recent trends of ceramic humidity sensors development: a review, Sens. Actuators B 228 (2016) 416–442.
[20] A.E. Souza, S.R. Teixeira, E. Longo, Titanatos: Fotoluminescência e Crescimento de Nanopartículas. (Titanates: Photoluminescence and Nanoparticles Growth), first ed., Saarbrüker, Germany, 2015.
[21] I.J. Langford, A.J.C. Wilson, Scherrer after sixty years: a survey and some new results in the determination of crystallite size, J. Appl. Crystallogr. 11 (1978) 102–113.
[22] D.L. Wood, J. Tauc, Weak absorption tails in amorphous semiconductors, Phys. Rev. B 5 (1972) 3144–3151.
[23] G. Narsimhan, Thermal decomposition of calcium carbonate, Chem. Eng. Sci. 16 (1961) 7–20.
[24] S.F.S. Mohamad, S. Mohamad, Z. Jemaat, Study of calcination condition on the composition of calcium carbonate in waste cockle shell to calcium oxide using thermal gravimetric analysis, J. Eng. Appl. Sci. (Faisalabad Pak.) 11 (2016) 9917–9921.
[25] K. Huang, L. Yuan, S. Feng, Crystal facet tailoring art in perovskite oxides, Inorg. Chem. Front. 2 (2015) 965–981.
[26] S. Kanagesan, M. Hashim, S. Jesurani, T. Kalaivani, I. Ismail, M.S.E. Shafie, Particle morphology and magnetic properties of $Ba_{0.5}Sr_{0.5}Fe_{12}O_{19}$ powder calcined conventionally and by microwave heating, J. Alloy. Compd. 543 (2012) 49–52.
[27] W.J. Park, M.K. Jung, T. Masaki, S.M. Im, D.H. Yoon, Characterization of YVO_4:Eu^{3+}, Sm^{3+} red phosphor quick synthesized by microwave rapid heating method, Mater. Sci. Eng. B 146 (2008) 95–98.
[28] A.P. Naumenko, N.I. Berezovska, M.M. Biliy, O.V. Shevchenko, Vibrational analysis and Raman spectra of tetragonal zirconia, Phys. Chem. Solid State. 9 (2008) 121–125.
[29] V.M. Orera, C. Pecharromán, J.I. Peña, R.I. Merino, C.J. Serna, Vibrational spectroscopy of $CaZrO_3$ single crystals, J. Phys.: Condens. Matter. 10 (1998) 7501.
[30] J.R. Ferraro, K. Nakamoto, C.W. Brown, Introductory Raman Spectroscopy, second ed., Elsevier Science, USA, 2003.
[31] C. Li, M. Li, UV Raman spectroscopy study on the phase transformation of ZrO_2, Y_2O_3-ZrO_2 and SO_4^{2-}/ZrO_2, J. Raman Spectrosc. 33 (2002) 301–308.
[32] P. Stoch, J. Szczerba, J. Lis, D. Madej, Z. Pedzich, Crystal structure and ab initio calculations of $CaZrO_3$, J. Eur. Ceram. Soc. 32 (2012) 665–670.
[33] X.L. Lovisa, Propriedade Fotoluminescente da ZrO2: Tb^{+3}, Eu^{+3}, Tm^{+3} Obtida Pelo Método de Polimerização de Complexos. (Photoluminescence Properties of ZrO_2: Tb^{+3}, Eu^{+3}, Tm^{+3} Obtained by polymerization of complexes) (Master's dissertation), Federal Universityof Rio Grande do Norte, Natal, Rio Grande do Norte, Brazil, 2013.